Changes in the vertical profile of the Indonesian Throughflow during Termination II: Evidence from the Timor Sea

Jian Xu,[1] Wolfgang Kuhnt,[1] Ann Holbourn,[1] Nils Andersen,[2] and Gretta Bartoli[1]

Received 26 January 2006; revised 31 May 2006; accepted 30 June 2006; published 13 October 2006.

[1] We use a multiproxy approach to monitor changes in the vertical profile of the Indonesian Throughflow as well as monsoonal wind and precipitation patterns in the Timor Sea on glacial-interglacial, precessional, and suborbital timescales. We focus on an interval of extreme climate change and sea level variation: marine isotope (MIS) 6 to MIS 5e. Paleoproductivity fluctuations in the Timor Sea follow a precessional beat related to the intensity of the Australian (NW) monsoon. Paired Mg/Ca and $\delta^{18}O$ measurements of surface- and thermocline-dwelling planktonic foraminifers (*G. ruber* and *P. obliquiloculata*) indicate an increase of >4°C in both surface and thermocline water temperatures during Termination II. Tropical sea surface temperature changed synchronously with ice volume (benthic $\delta^{18}O$) during deglaciation, implying a direct coupling of high- and low-latitude climate via atmospheric and/or upper ocean circulation. Substantial cooling and freshening of thermocline waters occurred toward the end of Termination II and during MIS 5e, indicating a change in the vertical profile of the Indonesian Throughflow from surface- to thermocline-dominated flow.

Citation: Xu, J., W. Kuhnt, A. Holbourn, N. Andersen, and G. Bartoli (2006), Changes in the vertical profile of the Indonesian Throughflow during Termination II: Evidence from the Timor Sea, *Paleoceanography*, *21*, PA4202, doi:10.1029/2006PA001278.

1. Introduction

[2] It has been increasingly recognized that tropical oceans, and in particular the Western Pacific Warm Pool (WPWP), play a fundamental role in modulating global climate change on interannual, millennial and orbital timescales [e.g., *Godfrey*, 1996; *Cane and Clement*, 1999; *Lea et al.*, 2000; *Koutavas et al.*, 2002; *Visser et al.*, 2003; *Medina-Elizalde and Lea*, 2005]. The Indonesian Throughflow (ITF) connects the upper water masses of the Pacific and Indian Oceans and substantially influences the salinity and heat exchange between these oceans [*Gordon and Fine*, 1996]. The annual mean heat transport of the ITF (about 1.15×10^{15} W) represents a heat sink for the Pacific Ocean and a major heat source for the Indian Ocean [*Schiller et al.*, 1998]. Today, the ITF transports an annual average ~16 Sv (1 Sv = 10^6 m^3 s^{-1}) of warm, low-salinity water from the WPWP and Indonesian-Malaysian archipelago into the eastern Indian Ocean [*You and Tomczak*, 1993; *Gordon and Fine*, 1996; *Schiller et al.*, 1998; *Gordon et al.*, 2003] (Figure 1). Warm water transported by the ITF amounts to 5.3 Sv of the total transport of 17.8 Sv in the upper branch of the global thermohaline Conveyor Belt at 20°N in the North Atlantic [*Speich et al.*, 2001]. Thus the ITF forms an important component of the global thermohaline circulation, and exerts a strong influence on regional as well as global climate. For instance, blockage of the ITF would depress the mean thermocline of the tropical Pacific and reduce the sea surface temperature (SST) difference between the WPWP and the eastern tropical Pacific cold tongue [*Lee et al.*, 2002].

[3] Today, the ITF is dominated by low-salinity, well-ventilated upper thermocline North Pacific water. North Pacific water mainly flows southward through the Sulawesi Sea into the Makassar Strait, and then follows two ways: one branch enters the Indian Ocean via the Lombok Strait (sill depth: 350 m) while the other branch mixes into the Flores Sea. Besides the Lombok Strait, there are two other main exit passages: the Ombai Strait (sill depth: 3250 m) and Timor Passage (sill depth: 1890 m). The mean transports through the three pathways obtained from mooring measurements are respectively 1.7 Sv [*Murray and Arief*, 1988], 5.0 ± 1 Sv [*Molcard et al.*, 2001] and 7.0 Sv [*Cresswell et al.*, 1993]. The modern ITF transport mainly occurs within the thermocline rather than at the sea surface. It has large seasonal and interannual variability with maximum annual average flow speeds between 50 and 100 m and important net flow down to 400 m water depth in the Makassar and Timor Straits [*Gordon et al.*, 1999; *Potemra et al.*, 2003]. Recent modeling work suggested that changes in the vertical profile of the ITF are more important to alter the stratification and surface heat fluxes of the Indian Ocean than mean transport flux [*Song and Gordon*, 2004] and that during glacials, thermocline flow was significantly reduced, whereas surface flow remained virtually unchanged [*Kuhnt et al.*, 2004; *Žuvela*, 2005].

[4] The hydrography of the WPWP region is strongly influenced by the semiannually reversed wind regime of the Asian-Australian monsoon and associated seasonal precipitation patterns. The Asian-Australian monsoon is a huge thermal circulation system driven by seasonal surface temperature differences between broadly central Asia and Australia [*Tapper*, 2002] (Figure 2). The east Asian boreal

[1] Institute of Geosciences, Christian-Albrechts-University, Kiel, Germany.
[2] Leibniz Laboratory for Radiometric Dating and Stable Isotope Research, Christian-Albrechts-University, Kiel, Germany.

0883-8305/06/2006PA001278

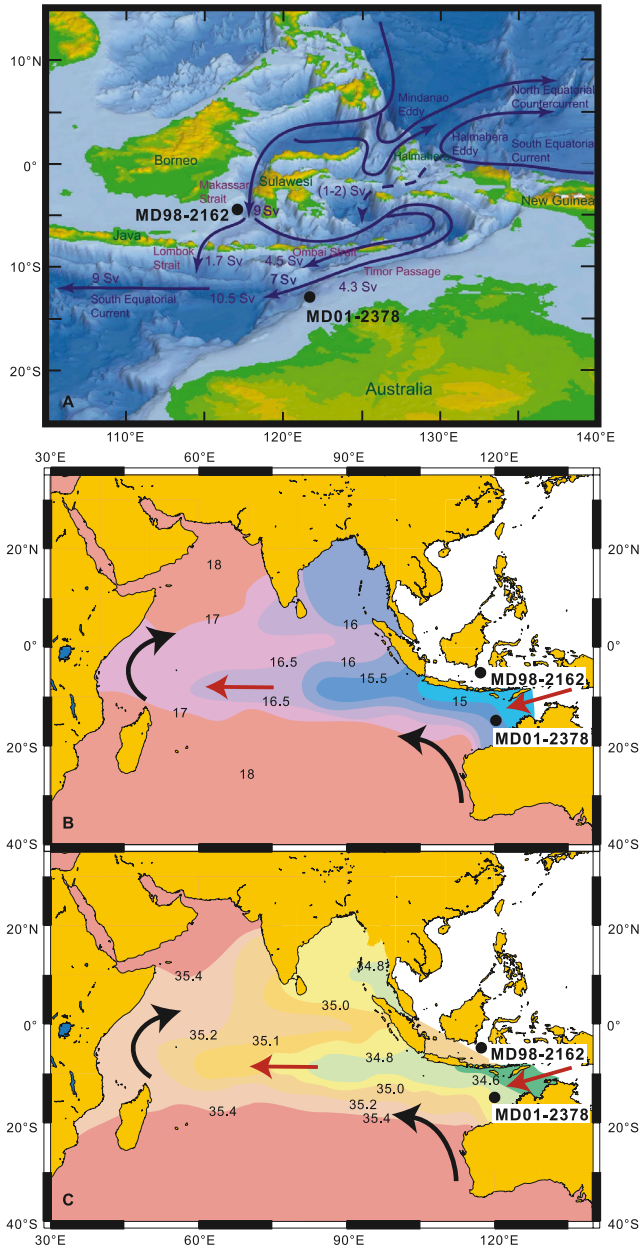

Figure 1. (a) Flow paths of present-day Indonesian Throughflow [after *Kuhnt et al.*, 2004] and Indian Ocean annual (b) mean temperature (°C) and (c) salinity in upper thermocline on isopycnal surface 25.7, located in the depth range 150–200 m [after *You and Tomczak*, 1993]. Arrows in Figures 1b and 1c indicate movement of Indian Central Water (black) and Australasian Mediterranean Water (red) derived from Indonesian Throughflow (ITF). Solid circles denote the locations of MD98-2162 and MD01-2378. Core MD01-2378 is situated in the frontal area between the two water masses.

winter (northeast) monsoon, which is in phase with the Australian austral summer (northwest) monsoon, is characterized by cold, dry air flowing southward across the South China Sea. In contrast, a moist northwest monsoonal flow becomes established over northern Australia during austral summer. The winds are relatively light in the monsoon transition periods of March–April and October–November, as the Intertropical Convergence Zone (ITCZ) moves alternatively north and south across the region [*Tapper*, 2002]. The ITCZ shift has substantial impact on the seasonal precipitation pattern over Australasia. While precipitation focuses in the north (South China Sea) and east (west Pacific) during boreal summer, a large part of the ITF area, including the eastern part of the Timor Sea and Timor Strait, receives high precipitation during the austral summer monsoonal season (December to March) [*Tapper*, 2002]. However, during glacial times, the southward shift of the ITCZ in boreal winter may have been considerably restricted, and/or the Australian summer monsoon may have been drier because of cooler Indian Ocean water masses (Figure 2).

[5] The main objectives of this work are to track changes in the vertical profile of the ITF outflow in the Timor Sea during a period of extreme climate change and sea level variation (Termination II) and to determine leads and lags in climatic, hydrographic and paleoproductivity proxies. We use a multiproxy approach to reconstruct temperature and salinity of surface and thermocline waters, and to investigate changes in the productivity driven particle flux to the deep ocean. Our work is based on high-resolution sediment

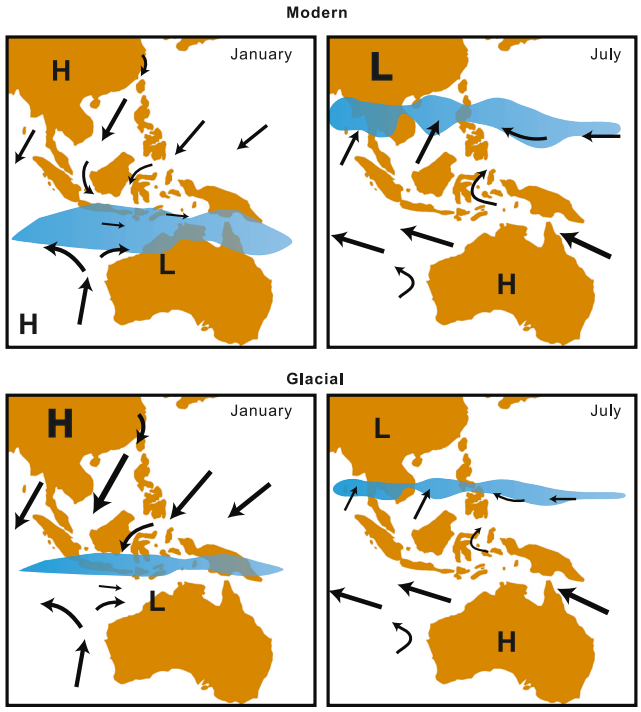

Figure 2. Modern and inferred glacial Australasian monsoon system. Main air pressure cells and wind-driven surface circulation are after *Wang et al.* [2005] and *Tapper* [2002]. Modifications for the glacial state include increased SE Asian winter monsoon and decreased SE Asian summer monsoon strength [*Jian et al.*, 2001], position of winter and summer Intertropical Convergence Zone closer to the equator with reduced precipitation [*De Deckker et al.*, 2002], and absence of surface water flow from South China Sea into Java Sea because of an exposed Sunda Shelf.

samples from IMAGES Core MD01-2378, recovered during the WEPAMA cruise in 2001, and complements an earlier investigation of the 40.73 m core in a time resolution of ~1–2 kyr [*Holbourn et al.*, 2005]. This previous study indicated that productivity fluctuations in the Timor Sea over the last 460 kyr were strongly influenced by monsoonal wind patterns offshore NW Australia (23 and 19 kyr variability), but were also modulated by sea-level-related variations in the intensity of the ITF (100 kyr variability) over glacial-interglacial cycles.

2. Material and Methods

[6] IMAGES Site MD01-2378 (13°4.95′S, 121°47.27′E; water depth: 1783 m) is located at the southern margin of the main outflow of the ITF in the Timor Sea (Figure 1). The sediment consists of undisturbed, homogenous, carbonate-rich nannoplankton ooze with abundant planktonic foraminifers and relatively rare benthic foraminifers. An initial age model was generated for the complete core, based on 21 AMS ^{14}C dates and 38 benthic oxygen isotope events [*Holbourn et al.*, 2005]. For the present study, sediment samples (~30–40 cc from 1 cm thick sediment slices) were taken at 1 cm distance in the interval 1310 to 1471 cm, corresponding to the transition from MIS 5e to MIS 6 according to the original age model. Samples were dried in an oven below 40°C, disaggregated by soaking in water, then wet sieved over a 63 μm screen. Residues were dried on a sheet of filter paper below 40°C, then sieved into 63–150 μm, 150–250 μm, 250–630 μm fractions.

2.1. Planktonic and Benthic Foraminiferal Census Counts

[7] Planktonic foraminifers were picked, identified and counted from an aliquot containing about 250 specimens in the size fraction >150 μm. The taxonomy follows *Bé* [1977] and *Saito et al.* [1981]. An average of 100–150 benthic foraminifers were picked, identified and counted in the size fraction >250 μm from every second sample. We used correspondence analysis to identify changes in faunal distribution following the approach in the work of *Holbourn et al.* [2005]. The initial counts of *Holbourn et al.* [2005] were included in the analysis. Census counts (normalized to individuals/gram sediment) of 84 species of benthic foraminifers in 81 samples were analyzed with CANOCO version 4.5 (output details given by *Ter Braak* [1995]). Since only sample scores on the first axis were used, no detrending was necessary. Rare species were downweighted during analysis. Resulting Factor I scores differ from *Holbourn et al.* [2005] in absolute values because of the different software used for analyses and the shorter stratigraphic interval analyzed. However, the major trends are preserved.

2.2. Stable Isotopes

[8] For the analysis of stable isotopes, we selected from all samples 20 tests of the surface water dweller *Globigerinoides ruber* (white), 8~10 tests of the subsurface dweller *Pulleniatina obliquiloculata* from the size fraction of 250~315 μm and 3 to 6 tests (>250 μm) of the epifaunal benthic foraminifer *Planulina wuellerstorfi* (except in a few samples, where *P. wuellerstorfi* was absent and *Cibicidoides mundulus* was analyzed). In a few samples, where benthic foraminiferal density was low, a smaller number (1–2) of specimens was analyzed. The initial isotopic data of *Holbourn et al.* [2005] were included. 16 replicate samples of *G. ruber* and *P. obliquiloculata* indicate that the mean reproducibility (1σ) is ±0.12‰ for δ^{18}O and ±0.13‰ for δ^{13}C. The mean reproducibility of 17 paired samples of *P. wuellerstorfi* is better than ±0.08‰ for δ^{18}O and δ^{13}C. Paired measurements on *P. wuellerstorfi* and *C. mundulus* indicate no significant offset between these two species.

[9] All tests were checked for cement encrustations and infillings before being broken into large fragments, then cleaned in alcohol in an ultrasonic bath and dried at 40°C. Stable carbon and oxygen isotope measurements were made with the Finnigan MAT 251 mass spectrometer at the Leibniz Laboratory, Kiel University. The instrument is coupled online to a Carbo-Kiel Device (Type I) for automated CO_2 preparation from carbonate samples for isotopic analysis. Samples were reacted by individual acid addition. The mean external error and reproducibility (1σ) of carbonate standards is better than ±0.07‰ and ±0.05‰ for δ^{18}O and δ^{13}C, respectively. Results were calibrated using the National Institute of Standards and Technology (Gaithersburg, Maryland) carbonate isotope standard NBS 20 and in addition NBS 19 and 18, and are reported on the Peedee belemnite (PDB) scale.

2.3. Mg/Ca Paleothermometry

[10] Mg/Ca ratios were measured on ~30 tests of *G. ruber* and *P. obliquiloculata*, from the same size fraction used for stable isotope analysis. To assess overall reproducibility, we duplicated measurements of 24 randomly selected samples. Foraminiferal tests, weighing about 0.2–0.8 mg per sample, were gently crushed under the microscope, and cleaned of contaminant phases using the standard foraminifera cleaning procedure with reductive step [*Martin and Lea*, 2002]. Samples were analyzed on an ICP-OES (Spectro Ciros SOP) with cooled cyclonic spray chamber and microconcentric nebulization (200 μL min^{-1}) at the Institute of Geosciences, Kiel University. Intensity ratio calibration followed the method of *de Villiers et al.* [2002]. Internal analytical precision from replicate measurements is better than 0.1–0.2% (relative standard deviation), which corresponds to ±0.02°C. Replicate analyses showed a standard deviation of 0.14 mmol/mol, equivalent to ±0.7°C. Consistency of results was checked by analyzing sets of standards obtained from M. Greaves, University of Cambridge. The validity of Mg/Ca ratio was checked by evaluating the consistency of Ca concentration before and after cleaning. Samples with a reduction in Ca concentration of more than 20% were rejected. Fe/Ca, Al/Ca and Mn/Ca ratios were additionally used to monitor cleaning efficacy, and samples with a significant correlation between Fe/Ca, Al/Ca, Mn/Ca and Mg/Ca values were excluded, following the method used by *Schmidt et al.* [2004]. As a result, 13 samples of *P. obliquiloculata* and 19 samples of *G. ruber* were discarded.

[11] SST was calculated from the Mg/Ca ratios of *G. ruber*, using the equation developed by *Anand et al.* [2003]. The equation, Mg/Ca = 0.38 (±0.02) exp 0.090 (±0.003) T, which yields an accuracy of ±1.2°C in estimating calcifica-

tion temperature, is based on the calibration of Mg/Ca in 12 species from sediment traps in the Sargasso Sea to $\delta^{18}O$-derived temperatures. In our core, this equation yielded identical SSTs compared to the species-specific equations for the tropical oceans employed by *Hastings et al.* [2001] and *Dekens et al.* [2002]. Thermocline water temperature derived from the subsurface dweller *P. obliquiloculata* Mg/Ca was based on a species-specific calibrated equation assuming an exponential constant of 0.09 [*Anand et al.*, 2003]. The equation is expressed as Mg/Ca = 0.328 (±0.007) exp 0.090 (±0.003)T. Termination II profiles of stable isotopes, Mg/Ca ratios and estimated temperatures at MD01-2378 are archived at WDC-MARE (http://www.pangaea.de, doi:10.1594/PANGAEA.472294).

[12] To assess validity of these equations in the region, foraminifera were picked from 12 multicore core top samples from six stations along a depth transect between 560 m and 2320 m including MD01-2378. These samples yielded average Mg/Ca values of 4.81 mmol/mol for *G. ruber* (n = 12, standard deviation: 0.25) and 2.38 mmol/mol for *P. obliquiloculata* (n = 12, standard deviation: 0.26). These values correspond to temperatures of 28.2° for *G. ruber* and 22.0° for *P. obliquiloculata*, which fall into the range of average summer SST (28°–29°C) and summer upper thermocline temperatures at 75–125 m water depth (22°–23°C) (World Ocean Atlas 2001 seasonal temperature data [*Conkright et al.*, 2002]). These data are archived at WDC-MARE (http://www.pangaea.de, doi:10.1594/PANGAEA.472296).

2.4. Salinity Reconstructions

[13] We calculated surface and thermocline water oxygen isotope composition ($\delta^{18}O_w$) from paired Mg/Ca and $\delta^{18}O$ measurements of *G. ruber* and *P. obliquiloculata*. We used the paleotemperature equation of *Bemis et al.* [1998] and *Thunell et al.* [1999]. This equation is expressed as $\delta^{18}O_w(\text{VSMOW}) = 0.27 + (T(°C) - 16.5 + 4.8 \times \delta^{18}O_{calcite}(\text{VPDB}))/4.8$. Using our core top data, a regional surface $\delta^{18}O_w$ value of −0.1‰ (±0.3) versus SMOW and an upper thermocline $\delta^{18}O_w$ of −0.3‰ (±0.2) versus SMOW are predicted. These values are intermediate between the measured $\delta^{18}O_w$ values of −0.5‰ in the WPWP water mass and 0.6‰ in the upper 300 m of the eastern Indian Ocean (Global Seawater Oxygen-18 Database (G. A. Schmidt et al., Goddard Institute for Space Studies, NASA, New York, 1999, available at http://data.giss.nasa.gov/o18data/, hereinafter referred to as Schmidt et al., Global Seawater Oxygen-18 Database, 1999)). Since $\delta^{18}O_w$ is corrected for the effect of temperature on the oxygen isotope fractionation between the foraminiferal test and water, $\delta^{18}O_w$ is only influenced by the change in $\delta^{18}O$ related to continental ice volume and local $\delta^{18}O$ variations related to the salinity of surface and thermocline water masses. As the $\delta^{18}O_w$ curves (bottom, thermocline and surface waters) carry the same ice volume signal, deviations mainly reflect changes in salinity.

2.5. Depth of Thermocline (DOT) Reconstructions

[14] Planktonic foraminiferal census data were used to estimate DOT, based on the transfer function developed by *Andreasen and Ravelo* [1997] for the tropical Pacific Ocean,

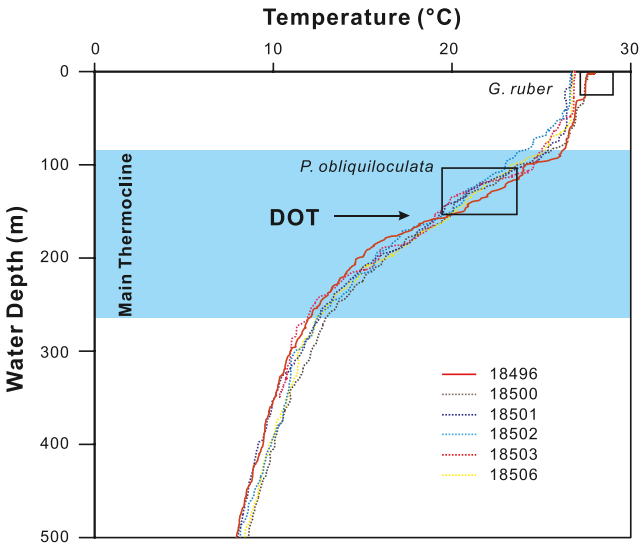

Figure 3. Definitions of mixed layer, thermocline, surface, and subsurface/thermocline waters. Depth ranges of *G. ruber* (0∼50 m) and *P. obliquiloculata* (∼100 m) from *Ravelo et al.* [1990] and *Anand et al.* [2003] are used to define "surface water" and "subsurface water" or "thermocline water." "Thermocline" is depth at which temperature changes most rapidly. Depth of thermocline (DOT) estimated from foraminiferal census data is equivalent to 18°C isothermal [*Andreasen and Ravelo*, 1997]. Temperatures and depths are from Sonne-185 conductivity-temperature-depth profiles acquired in late September 2005 at stations 18496, 18500, 18501, 18502, 18503, and 18506 in respective water depths of 2530, 1167, 742, 564, 354, and 2410 m [*Kuhnt et al.*, 2006]. Rectangles mark ranges of *G. ruber* and *P. obliquiloculata* Mg/Ca temperatures in 12 multicore core top samples.

where the 18°C isothermal is arbitrarily defined as the DOT. Today, the position of the 18°C isothermal in the Timor Sea is ∼170 m, corresponding to the depth range at which water temperature changes most rapidly (Figure 3). The equation has a standard error of ±22 m, and an additional ±5-m error is introduced by low species counts in the core top database. The DOT was also estimated from temperature differences between surface- and thermocline-dwelling species [*Anand et al.*, 2003]. *P. obliquiloculata* is considered to live below the mixed surface layer in thermocline waters, whereas *G. ruber* generally maintains a near-surface dwelling habitat [*Hemleben et al.*, 1989; *Ravelo and Fairbanks*, 1992]. Reported calcification depths for these two species are on the order of 100 m and 0–50 m, respectively [*Ravelo et al.*, 1990; *Anand et al.*, 2003], which is in agreement with measured Mg/Ca temperatures in core top samples (Figure 3). Thus the thermal gradient ($\Delta T_{(G.\ ruber\text{-}P.\ obliquiloculata)}$) increases, when DOT shallows, and decreases, when DOT deepens.

3. Results

3.1. Age Model

[15] The temporal resolution (∼1–2 kyr) of the original age model for Core MD01-2378 [*Holbourn et al.*, 2005] is

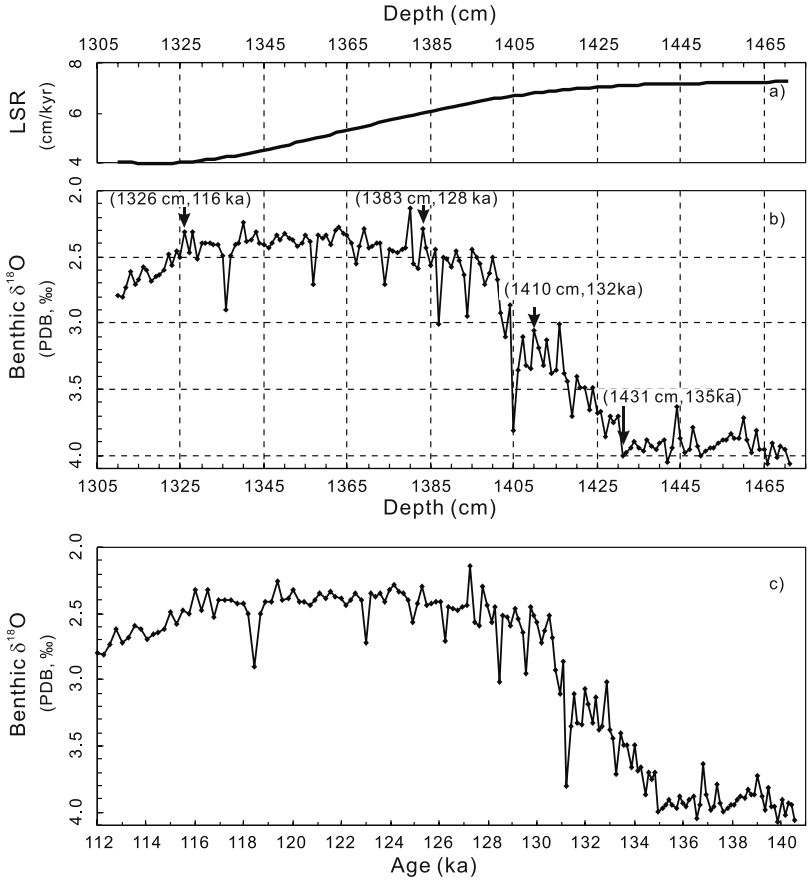

Figure 4. Age model for Termination II in Core MD01-2378. (a) Linear sedimentation rates (LSR) (cm/kyr). (b) Benthic δ^{18}O (PDB, ‰) versus depth. Arrows indicate age tie points following *Shackleton et al.* [2002, 2003] and *Martinson et al.* [1987]. (c) Benthic δ^{18}O versus age.

too low to be applied to Termination II. Thus we developed a new age model for MIS 6–5e, which follows the specific benthic oxygen isotope stratigraphy for MIS 5e at MD95-2042 (37°48′N, 10°10′W; water depth: 3146 m) in the work of *Shackleton et al.* [2002, 2003]. Our benthic δ^{18}O curve closely resembles the MD95-2042 curve for the interval MIS 6–5e, showing a distinct plateau between 1326 and 1400 cm. This plateau was assigned an age of 116–128 ka by *Shackleton et al.* [2002, 2003] using radiometric dates of marine coral terraces corresponding to the MIS 5e sea level highstand. While the end (116 ka) of the MIS 5e plateau is quite distinct at 1326 cm in our δ^{18}O curve, the onset of the plateau (128 ka) is somewhat ambiguous (Figure 4). Low δ^{18}O values of 2.5‰ already occur at 1400–1385 cm, but consistent δ^{18}O values around 2.4‰ are only reached at 1383 cm. We selected this latter point as the onset of the MIS 5e plateau, as the thermocline species *P. obliquiloculata* also exhibits a marked decrease in δ^{18}O of more than 1‰ between 1400 cm and 1385 cm.

[16] The midpoint of the MIS 6–5e transition was correlated with the sea level stillstand of −60 to −80 m, dated at 132 ± 2 ka in the "Alladin's Cave" record [*Esat et al.*, 1999; *Shackleton et al.*, 2003]. We correlate this sea level stillstand with the small δ^{18}O plateau between 1406 and 1417 cm, corresponding to 12 data points, with an average value of 3.24‰ and ∼1.4‰ standard deviation. The midpoint of the plateau at 1410 cm was correlated to the Alladin's Cave event. Event 6.1 at 1431 cm in our core, was determined at 135 ka following *Martinson et al.* [1987], as no revised age was proposed by *Shackleton et al.* [2002, 2003].

[17] To construct our age model, a smooth curve was fitted using locally weighted (10% of data) least squares (Stineman function) to tie points at 135 ka (1431 cm), 132 ka (1410 cm), 128 ka (1383 cm) and 116 ka (1326 cm), then the interpolated curve was sampled. For the few samples above 1326 cm we assumed that sedimentation rate remained consistent. For the interval below 1431 cm, we used the well-defined MIS 6.5 as additional tie point [*Holbourn et al.*, 2005]. The interval between 1471 and 1310 cm then covers 140.6∼112 ka and the average temporal sampling resolution is about 200 yr. Sedimentation rates vary between 4 and 4.5 cm/kyr during MIS 5e and between 6 and 7.5 cm/kyr during MIS 6 (Figure 4), which appears much lower than a rate of 19 cm/kyr during the last 30 kyr [*Holbourn et al.*, 2005]. However, the high sedimentation rate in the upper part of the core is artificial because of the Calypso coring technique.

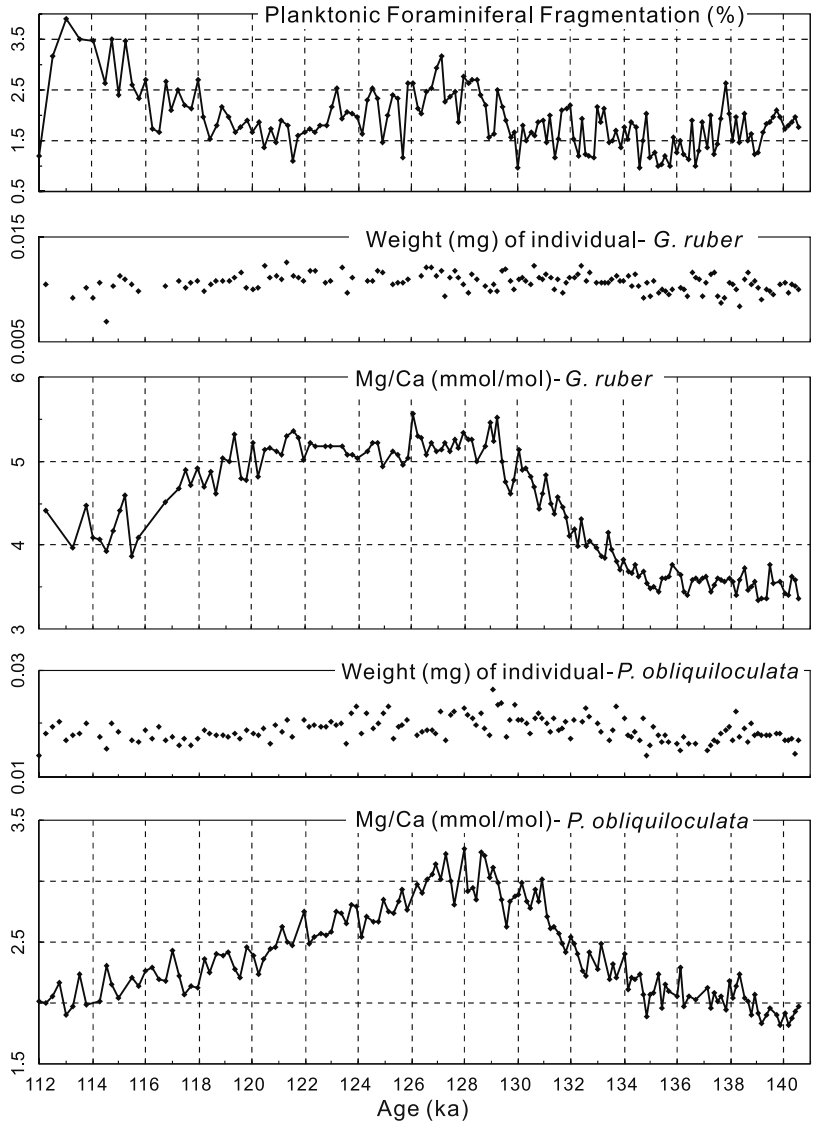

Figure 5a. Impact of carbonate dissolution on Mg/Ca in *G. ruber* and *P. obliquiloculata*. Comparison of planktonic foraminiferal fragmentation index calculated from (fragments/8)/(fragments/8 + whole tests) × 100%, weight of individual shells (mg), and Mg/Ca ratio (mmol/mol).

3.2. Surface and Subsurface Water Temperature Reconstructions Based on Mg/Ca

3.2.1. Dissolution Effects on Mg/Ca Measurements

[18] Dissolution can result in underestimated temperatures through selective dissolution of Mg-rich portions in foraminiferal tests [*Lea et al.*, 2000; *Rosenthal et al.*, 2000; *Dekens et al.*, 2002; *Rosenthal and Lohmann*, 2002; *Russell et al.*, 2004]. Dissolution occurs approximately 2000 m above the foraminiferal lysocline, and even well-preserved tests may be severely dissolved [*Lohmann*, 1995].

[19] Several lines of evidence indicate that calcite is well preserved in our samples and that Mg/Ca ratios are not significantly biased by partial dissolution. First, Site MD01-2378 (1783 m water depth) is located ~2000 m above the present lysocline. Secondly, planktonic foraminiferal fragmentation (calculated from the relation: (fragments/8)/(fragments/8 + whole tests) × 100%), which provides a reliable dissolution index [*Le and Shackleton*, 1992; *Conan et al.*, 2002], is low with an average of 1.9%, and highest value of only 3.9% at 115.1 ka (Figure 5a). In addition, the weight of individual tests remains consistent in both *G. ruber* (average 0.0107 ± 0.0009 mg per individual) and *P. obliquiloculata* (0.0190 ± 0.0025 mg), and no significant correlation is apparent between Mg/Ca values and shell weights in glacial (MIS 6) and interglacial (MIS 5e) periods (Figure 5b). Correlation coefficients (R^2) are 0.097 and 0.069 for *G. ruber*, and 0.168 and 0.065 for *P. obliquiloculata* during MIS 5e and 6, respectively.

3.2.2. Mg/Ca in *G. ruber* and *P. obliquiloculata*

[20] Mg/Ca ratios in *G. ruber* range from 3.34 to 5.56 mmol/mol and in *P. obliquiloculata* from 1.82 to 3.26 mmol/mol (Figure 5a). These ratios are within the ranges of average intra-annual variations in sediment traps observed by *Anand et al.* [2003]. The highest values occur

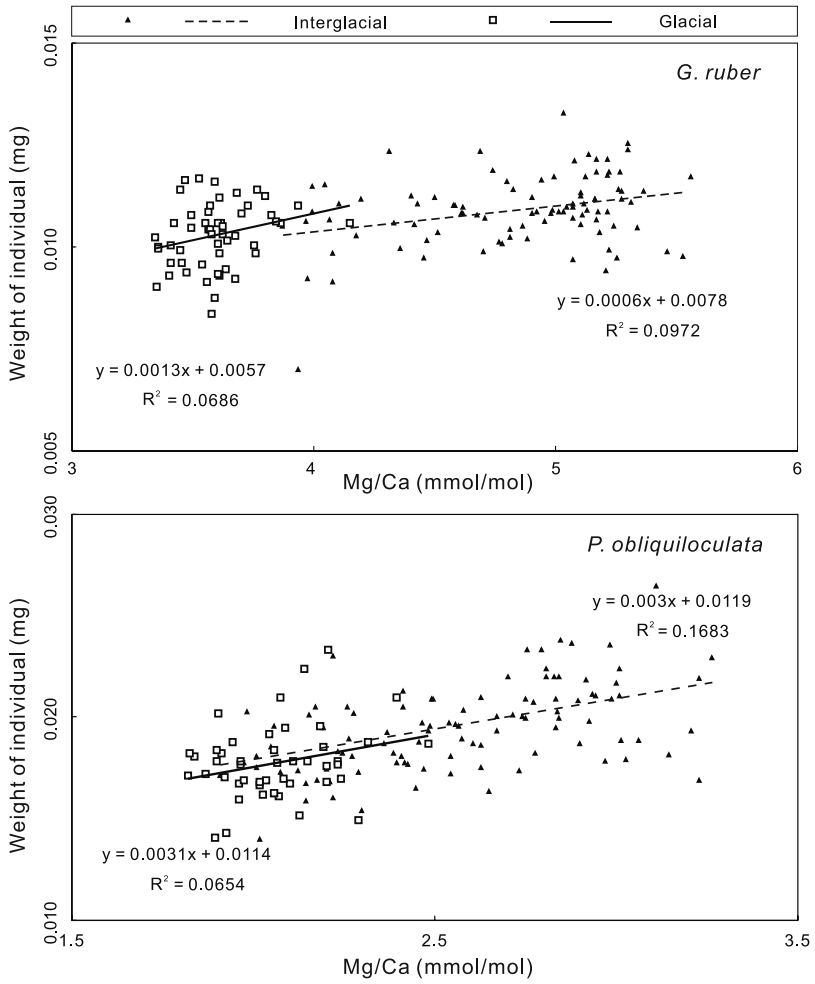

Figure 5b. Linear regression of shell weight versus Mg/Ca ratio in *G. ruber* and *P. obliquiloculata* over interglacial (132–114.7 ka) and glacial (143.2–132.2 ka) intervals.

in MIS 5e, at 126 and 128 ka. The lowest value for *G. ruber* is at 139.1 ka and for *P. obliquiloculata* at 140.2 ka. Two striking features of the *G. ruber* curve are the plateaux in MIS 6 (3.54 ± 0.10 mmol/mol between 140.6 and 135.4 ka) and in MIS 5e (5.19 ± 0.14 mmol/mol during 129.3∼118.9 ka interval). In contrast, the Mg/Ca ratios of *P. obliquiloculata* increase sharply until 128 ka, then decrease gradually (Figure 5a).

3.2.3. Temperature Reconstructions

[21] Figure 6 shows estimates of calcification temperatures for *G. ruber* and *P. obliquiloculata* based on Mg/Ca ratios. *G. ruber* has been suggested as the most accurate recorder of SST by *Dekens et al.* [2002]. *G. ruber* shows highest SST (29.8°C) at 126 ka, within the "plateau" of MIS 5e, and lowest SST (24.2°C) at 139.1 ka. The average estimated glacial SST between 140.6 and 135.4 ka is 24.8°C ± 0.3°C, and the average SST within the MIS 5e "plateau" (128–116 ka) is 28.8 ± 0.4°C (Figure 6). The mean temperature difference and the difference between maximum and minimum in these two intervals are 4.2°C and 5.6°C, respectively. These glacial-interglacial SST differences are comparable to the values of 4.1 ± 0.6°C and 5.3 ± 0.7°C estimated by *Visser et al.* [2003] for Site MD98-2162 in the Makassar Strait (4°41.33′S, 117°54.17′E; 1855 m water depth; Figure 1).

[22] *P. obliquiloculata* Mg/Ca-based thermocline water temperatures (ranging from 19°C to 25.5°C) are on average lower by ∼4°C than *G. ruber* surface temperatures. Calcification temperature estimates for *P. obliquiloculata* increase from ∼19° at 140.6 ka to ∼25° at 128 ka, then decrease to ∼19.5°C at 113 ka (Figure 6). It is also striking that both *G. ruber* and *P. obliquiloculata* Mg/Ca-based temperatures show a sudden cooling of ∼1°C at ∼129.5 ka, just before temperatures reach their highest values at the end of Termination II.

3.3. Surface and Subsurface Salinity Changes ($\delta^{18}O_w$)

[23] Sea surface and upper thermocline $\delta^{18}O_w$ remain high (around 1‰ versus SMOW) until ∼130 ka, whereas the ice-volume-related component of $\delta^{18}O_w$ started to decrease at ∼135 ka (Figure 7). This difference to the global trend probably stems from the high salinity of surface and upper thermocline waters in the early part of Termination II, related to low regional precipitation and high evaporation. A steep decrease in thermocline $\delta^{18}O_w$

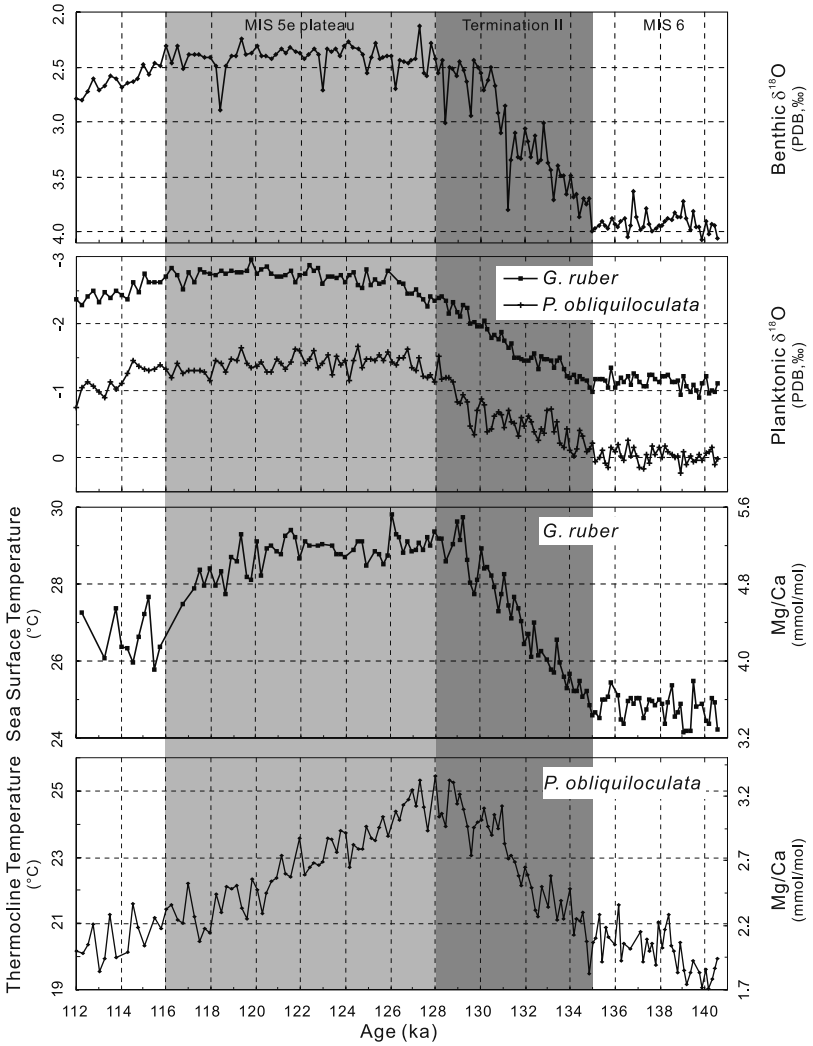

Figure 6. Comparison of benthic and planktonic $\delta^{18}O$ (PDB, ‰), sea surface temperature (estimated from *G. ruber* Mg/Ca), and subsurface water temperature (estimated from *P. obliquiloculata* Mg/Ca). Definitions of surface and subsurface waters are given in Figure 3 caption. Darker shading marks Termination II (135–128 ka), and lighter shading marks MIS 5e plateau (128–116 ka).

begins at ~130 ka and is maintained throughout the MIS5e plateau indicating freshening of thermocline waters. The difference in thermocline $\delta^{18}O_w$ between the early part of Termination II and the late part of MIS 5e exceeds 1.5‰, which is significantly more than the ice volume effect of ~1‰ [*Waelbroeck et al.*, 2002]. Surface water $\delta^{18}O_w$ during Termination II and early MIS 5e is within the range of the ice volume effect, but shows a phase lag of approximately 3 kyr, which probably relates to delayed freshening.

3.4. Depth of Thermocline (DOT)

[24] DOT estimates for Termination II in Core MD 01-2378 are shown in Figure 8. The DOT curve exhibits a sinuoidal pattern, with a flat valley between 135~128 ka. The average DOT is 162 ± 16 m during MIS 5e (128~112 ka), 159 ± 12 m during MIS 6 (140.6~135 ka) and ~175 m during Termination II. The present-day DOT position, which is constrained by the 18°C isotherm [*Andreasen and Ravelo*, 1997], is at ~170 m in our core [*Bassinot et al.*, 2002; *Kuhnt et al.*, 2006]. Therefore DOT estimates are close to the modern 18°C isotherm depth (~170 m). Variations in ΔT are consistent with fauna-based DOT estimates, except for the latest part of MIS 5e, when both estimates exhibit high-frequency variations.

3.5. Paleoproductivity Proxies

[25] Accumulation rates of benthic foraminifers show a linear correlation to food resources and thus to digestible export flux at the seafloor [*Herguera and Berger*, 1991]. However, they may be influenced by high-frequency fluctuations in sedimentation rates related to sediment focusing, winnowing or current-related rapid sedimentation events. In Core MD01-2378, benthic foraminiferal accumulation rates decrease from ~50 to ~20 specimens/cm^2/kyr during the transition from MIS 6 to 5e (135–131 ka), remained at ~20 until 122 ka before steadily increasing

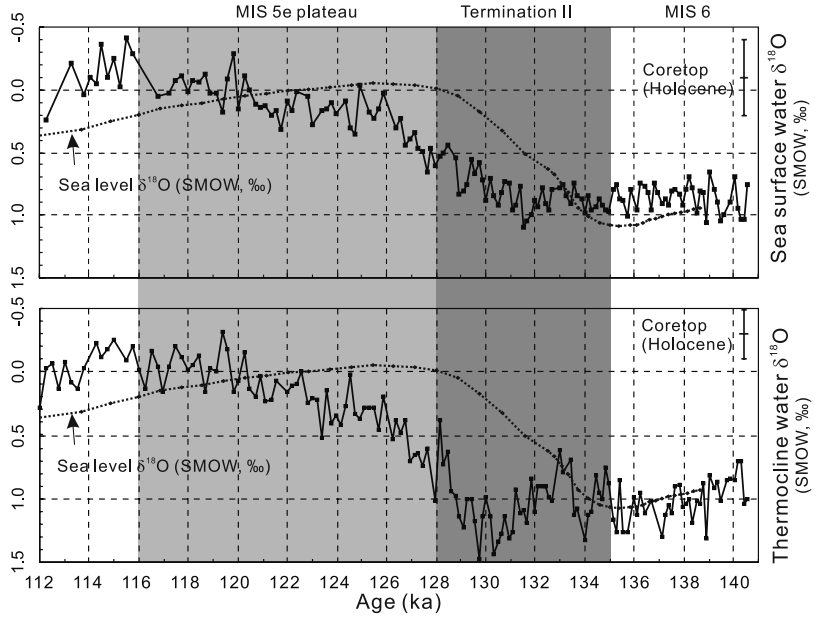

Figure 7. Comparison of estimated surface and thermocline water δ^{18}O (SMOW, ‰). Water δ^{18}O was calculated using the equation of $\delta^{18}O_w(\text{VSMOW}) = 0.27 + (T(°C) - 16.5 + 4.8 \times \delta^{18}O_{calcite}(\text{VPDB}))/4.8$ of *Bemis et al.* [1998]. Ice-volume-related δ^{18}O changes are from *Waelbroeck et al.* [2002], adjusted to the age model for MIS 6 and 5e [*Shackleton et al.*, 2003]. Range of modern $\delta^{18}O_w$ calculated with the same method is indicated by an error bar in each plot (derived from multicore core top samples of station MD01-2378 and five additional stations in the vicinity). These values are well within the range of measured modern $\delta^{18}O_w$ of approximately −0.5‰ for low-salinity Western Pacific Warm Pool water and +0.6‰ for eastern Indian Ocean surface water (Schmidt et al., Global Seawater Oxygen-18 Database, 1999).

from ∼20 (at 122 ka) to ∼60 specimens/cm^2/kyr (at 113 ka) (Figure 9). The productivity index based on F1 values derived from correspondence analysis takes into account the distribution of species within assemblages, and is less sensitive to changes in sedimentation rate. This index is generally strongly correlated to the export flux at the seafloor [*Kuhnt et al.*, 1999; *Wollenburg and Kuhnt*, 2000].

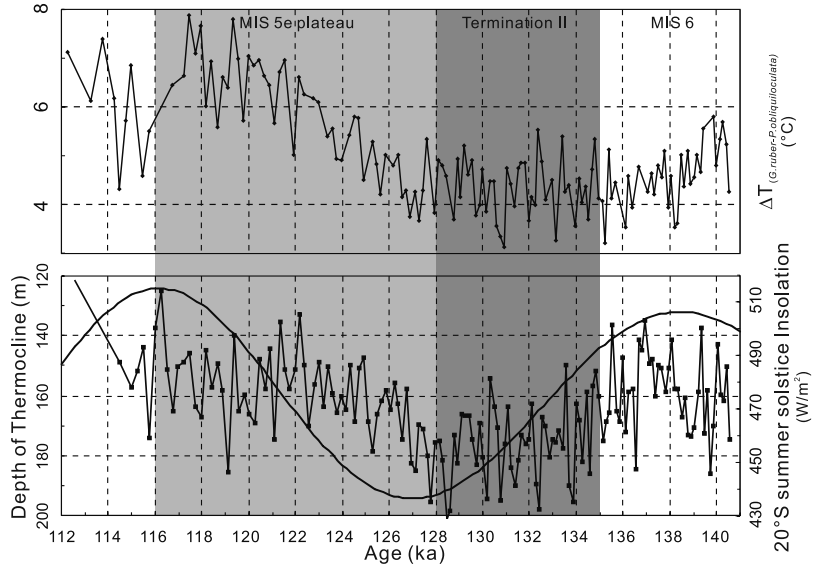

Figure 8. Comparison of DOT estimated from planktonic foraminiferal transfer function [*Andreasen and Ravelo*, 1997] and thermal gradient between surface and subsurface waters ($\Delta T_{(G.\ ruber\text{-}P.\ obliquiloculata)}$) with 20°S summer solstice (austral) insolation. Insolation curve derived from "ANALYSERIES" [*Paillard et al.*, 1996] based on orbital solution of *Laskar* [1990].

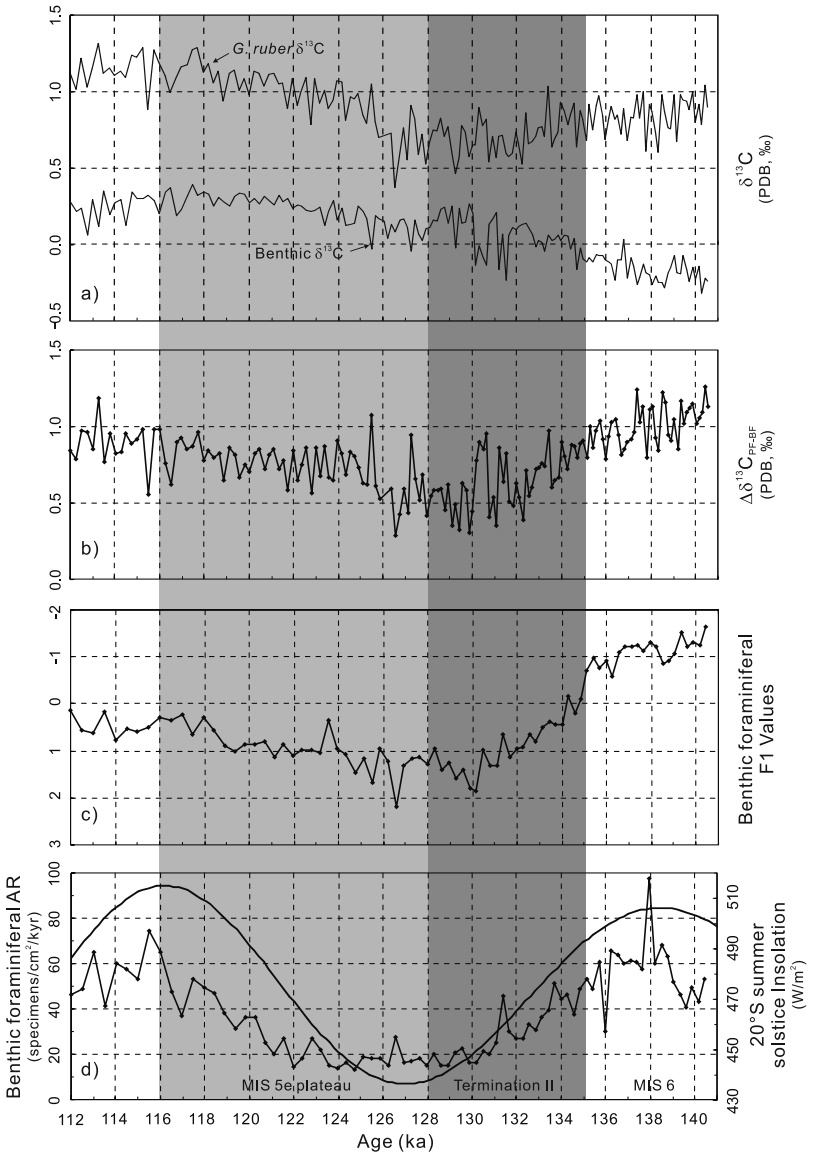

Figure 9. (a) Comparison of δ^{13}C of *G. ruber* and benthic δ^{13}C. The δ^{13}C difference between (b) planktonic and benthic foraminifers ($\Delta\delta^{13}C_{PF\text{-}BF}$), (c) benthic foraminiferal F1 values, and (d) accumulation rates with 20°S summer solstice (austral) insolation.

[26] The difference in δ^{13}C between planktonic and benthic foraminifers ($\Delta\delta^{13}C_{(PF\text{-}BF)}$) has also been used for qualitative estimates of export productivity in tropical and subtropical oceans [*Sarnthein and Winn*, 1990; *Jian et al.*, 2001]. However, owing to the complexity of factors influencing δ^{13}C, this index needs to be evaluated in combination with other export flux proxies. In Core MD01-2378, the $\Delta\delta^{13}C_{(PF\text{-}BF)}$ curve bears similarity to the productivity index based on benthic foraminiferal census counts (Figure 9), and thus is probably related to productivity changes in near-surface waters.

4. Discussion

4.1. Stepwise Deglaciation

[27] The small plateaux in the benthic δ^{18}O record of Core MD01-2378 (Figure 6), centered at approximately 132 ka (Alladin's Cave event [*Shackleton et al.*, 2003]) and 130 ka ("Younger Dryas II" [*Cortese and Abelmann*, 2002]), indicate a stepwise deglaciation during Termination II. Each plateau ends with a short increase in δ^{18}O values, suggesting transient cooling of deep-intermediate water or ice expansion. Whereas the "Alladin's Cave event" is not reflected in tropical SST in Core MD01-2378, our planktonic data suggest that surface cooling also occurred during the Younger Dryas II event at 129.5 ka (Figure 6). The sudden decrease in SST and thermocline temperatures by ~1°C at the end of Termination II (129.5 ka) is reminiscent of the Younger Dryas cooling event during Termination I. The Younger Dryas II event was previously recognized in ODP Site 1089 in the South Atlantic [*Cortese and Abelmann*, 2002], and may represent a global event related to perturbations of the thermohaline circulation

related to meltwater pulses, as was proposed for the Younger Dryas event.

[28] It is also striking that the MIS 5e plateau is marked by increases in benthic δ^{18}O at 126.2, 124.9, 123 and 118.5 ka (Figure 6). The most striking increase at 118.5 ka seems to correspond to the cooling event in the Southern Ocean at 118.5 ka [*Cortese and Abelmann*, 2002], in the north Greenland ice core at 119 ka [*North Greenland Ice Core Project Members*, 2004], and to the global sea level drop at 118 ka [*Lambeck and Chappell*, 2001, Figure 3] and late Eemian aridity pulse at 118 ka [*Sirocko et al.*, 2005]. However, it is difficult to ascertain whether the δ^{18}O increase at 118.5 ka in Core MD01-2378 refers indeed to a global event, since the other records considered above are based on different age models.

4.2. Sea Level and Monsoonal Controls on Timor Sea Hydrography

4.2.1. Glacial-Interglacial Change in ITF Vertical Profile

[29] Seawater oxygen isotope reconstructions based on paired Mg/Ca and δ^{18}O measurements of surface- and thermocline-dwelling planktonic foraminifers indicate high salinity in surface and thermocline waters during MIS 6 and the early part of Termination II (Figure 7), pointing to the strong influence of Indian Ocean intermediate water in the Timor Sea. A decrease in surface water δ^{18}O, started around 132 ka (the Alladin's Cave event or midpoint of the MIS 6 to 5e transition), implying increased flow of warm, fresh surface water from an expanding WPWP. The freshening of thermocline water, coinciding with the Younger Dryas II event (129.5 ka) started later, indicating delayed strengthening of thermocline flow. Interestingly at that time, the rising sea level must have reached the threshold water depth of -50 to -60 m, allowing a marine connection to be established between the South China Sea and Java Sea. Such a connection would have promoted the establishment of a freshwater pool at the southern end of the Makassar Strait, which inhibited surface outflow and promoted thermocline outflow from the Makassar Strait, in a similar fashion to the present day [*Gordon et al.*, 2003].

[30] Lowered sea level and restricted passages remained a major control on ITF vertical structure during MIS 6 and most of Termination II. Modeling experiments also suggest that during glacial sea level lowstands ITF intensity decreased and the ITF vertical structure changed toward increased surface flow relative to thermocline flow [*Žuvela*, 2005]. Contributing mechanisms would be (1) strengthened NE Asian winter monsoon increasing surface flow in the Makassar Strait (the main passage of the ITF) and (2) unrestricted surface outflow from the Makassar Strait during NE Asian winter monsoon, since fresh water entering from the Java Sea, which today obstructs surface circulation at the southern end of the Makassar Strait [*Gordon et al.*, 2003], was suppressed, when the Sunda Shelf was exposed during sea level lowstands.

[31] Substantial deepening of the thermocline occurred during Termination II in the Timor Sea (Figure 8). However, it is somewhat surprising that the DOT reached its deepest position just before the beginning of the MIS 5e plateau, and was comparatively shallow during both MIS 6 and MIS 5e (Figure 8). Deepening of the thermocline in the early part of Termination II probably stemmed from increased surface flow, before a marine connection existed between the South China Sea and Java Sea. A reduced glacial ITF would explain thermocline shallowing during MIS 6, but cannot account for the shallowing during MIS 5e. Modeling experiments and oceanographic measurements indicate that today the ITF transport is stronger within the thermocline than at the surface [*Gordon et al.*, 2003; *Song and Gordon*, 2004]. An increase in cool, fresh thermocline flow, resulting in a vertical profile similar to that of the modern ITF, would explain shoaling of the thermocline in the Timor Sea in the latest part of Termination II and MIS 5e.

4.2.2. Monsoonal Influence on Paleoproductivity

[32] Modern seasonal productivity patterns along the NW Australian margin are strongly influenced by intrusions of cool, nitrate-rich slope waters below the warm, low-salinity surface layer during austral summer, when the surface ITF is weak and the Leeuwin current is relaxed, resulting in a comparatively shallow pycnocline. These intrusions result in intense deep chlorophyll maxima since the solar radiation is strong enough to sufficiently illuminate subpycnocline water for algal growth [*Longhurst*, 1998]. Additionally, mixing of the surface layer by cyclones, which occurs frequently offshore NW Australia during the austral summer monsoon season [*Tapper*, 2002], contributes to increased productivity.

[33] The strength of the Australian (NW) monsoon thus influences the upper water column in the Timor Sea by intensifying vertical mixing of the surface layer and promoting the reversing of currents in December–February. The effect of the Australian monsoon was detected in the productivity record of the Timor Sea, which revealed a marked precessional response over the last 460 kyr [*Holbourn et al.*, 2005]. The high-resolution benthic foraminiferal paleoproductivity proxy record over Termination II also follows closely summer insolation variations over NW Australia. A strong decrease in marine productivity is evident at ~138 ka with a minimum at the onset of MIS 5e (128 ka), which is followed by a slight recovery during MIS 5e (Figure 9). Paleoproductivity fluctuations in the Timor Sea appear linked to the waxing and waning of monsoonal winds and associated changes in vertical mixing and currents. An additional effect of strengthened Australian monsoon may be the blockage of warm surface outflow from the Timor Strait, which would lead to thermocline shoaling in the Timor Sea and promote local upwelling of nutrient-rich Indian Ocean intermediate water.

4.3. Phasing of Ice Volume Change and Tropical SST: High- Versus Low-Latitude Climate Change

[34] The MD01-2378 SST record, based on Mg/Ca of *G. ruber,* reveals a rise of ~4°C in the Timor Sea during Termination II, which has similar magnitude as the increase detected in Core MD98-2162 from the Makassar Strait [*Visser et al.*, 2003]. In Core MD01-2378, the temperature rise is coeval with the first decline in benthic δ^{18}O at ~135 ka marking the onset of Termination II, and a "plateau" in SST (~29°–30°C) is sustained between 129 and 118 ka

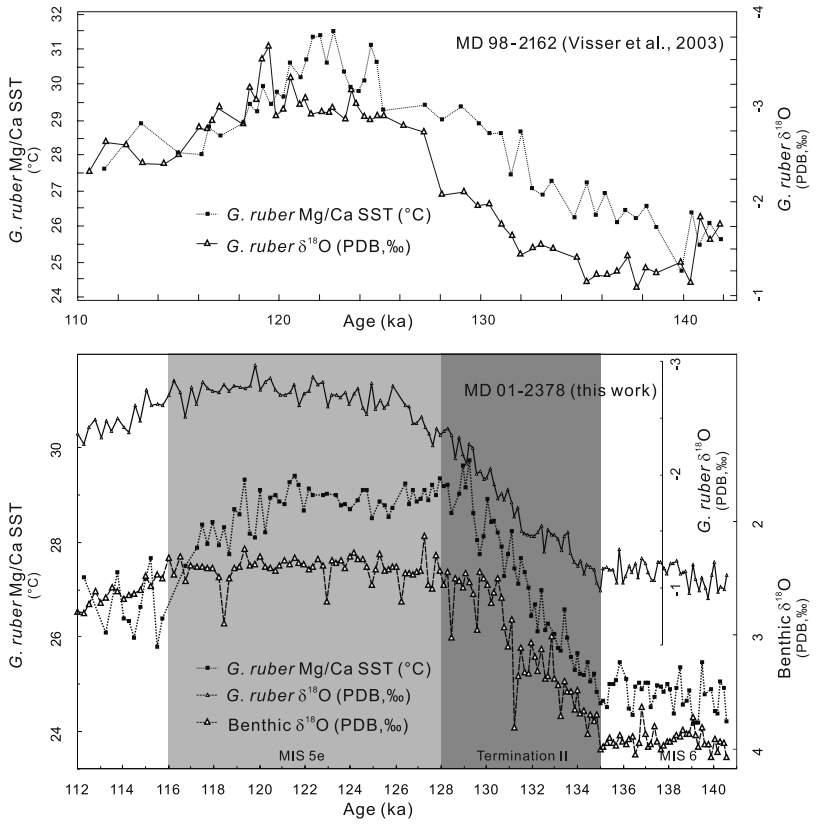

Figure 10. Phase relations between SST and $\delta^{18}O$ during Termination II. (bottom) Tropical SST changes synchronously with ice volume and leads planktonic $\delta^{18}O$ in Core MD01-2378. (top) In contrast, SST leads planktonic $\delta^{18}O$ in Core MD98-2162 from the Makassar Strait [*Visser et al.*, 2003].

(Figure 6). However, at these two locations, there is a fundamental difference in the phasing between SST and planktonic $\delta^{18}O$ (Figure 10). In the Timor Sea, SSTs are in phase with both planktonic and benthic $\delta^{18}O$ until the beginning of MIS 5e. In contrast, SSTs lead planktonic $\delta^{18}O$, interpreted as global ice volume, by 2∼3 kyr in the Makassar Strait [*Visser et al.*, 2003]. However, since no benthic $\delta^{18}O$ data are available for the Makassar Strait, the interpretation of the $\delta^{18}O$ record remains ambiguous. A lead of tropical SST to ice volume was also reported from the equatorial Pacific by *Lea et al.* [2000], spurring an intense debate about the role of the tropics in past global climate change. Pacific tropical SST records lead continental ice volume by ∼3 kyr [e.g., *Lea et al.*, 2000; *Koutavas et al.*, 2002; *Visser et al.*, 2003; *Medina-Elizalde and Lea*, 2005], but coincide with changes in Antarctic air temperature [*Lea et al.*, 2000]. In contrast, Atlantic records suggested that tropical SST changed synchronously with Northern Hemisphere high-latitude climate and ice sheet response [*Lea et al.*, 2003].

[35] These discrepancies may to some extent be explained by local variability in tropical climate, mainly stemming from monsoonal systems and seasonal migration of the ITCZ [*Lea et al.*, 2003], seasonal proxy bias during cool glacial periods or proxy noise masking a small early rise of sea level [*Ashkenazy and Tziperman*, 2006]. A lag of planktonic $\delta^{18}O$ to both SST and benthic $\delta^{18}O$ was recently reported from the northern South China Sea where surface water hydrography is strongly affected by the east Asian summer monsoon [*Oppo and Sun*, 2005]. These authors suggested a strong influence of summer monsoon intensity on sea surface salinity and surface water $\delta^{18}O$ by large-scale redistribution of $\delta^{18}O$ depleted rainfall from land to sea when the monsoon weakens. The Makassar Strait record is likely influenced by changes in local monsoonal precipitation, since surface salinity at this location is strongly influenced by local rainfall and continental runoff from Borneo. A lag of surface $\delta^{18}O_w$ to SST at glacial terminations could be related to decreasing monsoonal rainfall over Borneo associated with a northward shift of the ITCZ during the boreal summer with strong repercussion on surface salinity and $\delta^{18}O_w$ in the early phase of the glacial termination. In Core MD01-2378, the synchroneity of SST and benthic $\delta^{18}O$ supports that ^{16}O-enriched water from melting ice sheets reached the Timor Sea when warming started in the tropics, indicating an almost instantaneous heat transfer between high and low latitudes. Synchronous warming of SE Asian tropical-subtropical seas and melting of continental ice sheets is also reported from several sites in the South China Sea and support the notion of a strong atmospheric connection between high northern latitudes and SE Asia [*Kienast et al.*, 2001; *Oppo and Sun*, 2005]. A high-latitude influence on tropical SST was also detected in long-term Pleistocene records from the eastern equatorial

Pacific, which revealed a strong obliquity component in tropical SST [*Liu and Herbert*, 2004]. According to these authors, tropical SST lead ice volume at the obliquity band, but are in phase with high-latitude insolation, indicating a direct coupling between low and high latitudes via the atmosphere or/and upper ocean.

5. Conclusion

[36] Sediment samples taken at 1 cm interval in Core MD01-2378, located at the northwestern margin of the Scott Plateau in the Timor Sea, were analyzed to reconstruct temperature and salinity in surface and thermocline waters and paleoproductivity fluctuations during Termination II. Our study reveals changes in the vertical profile of the ITF as well as monsoonal wind and precipitation patterns in the Timor Sea on glacial-interglacial, precessional and suborbital timescales.

[37] Paleoproductivity fluctuations in the Timor Sea follow a precessional beat related to the intensity of the Australian (NW) Monsoon with maxima at 138 ka (MIS 6) and 116 ka (end of MIS 5e). Paired Mg/Ca and $\delta^{18}O$ measurements of surface- and thermocline-dwelling planktonic foraminifers (*G. ruber* and *P. obliquiloculata)* indicate an overall increase of >4°C in both SST and thermocline water temperature over Termination II. Surface flow increased at the onset of Termination II, whereas thermocline flow was still restricted, and thermocline waters in the Timor Sea remained strongly influenced by relatively saline Indian Ocean intermediate water. Lowered sea level and restricted passages exerted a major control on ITF vertical structure during the onset of Termination II.

[38] Substantial cooling and freshening of thermocline waters during MIS 5e indicate a change in the vertical profile of the Indonesian Throughflow from surface to thermocline-dominated flow, possibly related to restricted surface flow through the southern exit of the Makassar Strait. In contrast, SST exhibits a distinct plateau during most of the MIS 5e sea level highstand indicating the persisting influence of a stable WPWP. Tropical SST changed synchronously with ice volume (benthic $\delta^{18}O$) during deglaciation, implying a direct coupling of high- and low-latitude climate via atmospheric and/or upper ocean circulation.

[39] **Acknowledgments.** We thank Yair Rosenthal, Arnold Gordon, and Lowell Stott for helpful discussions and Robert Thunell for providing Mg/Ca and $\delta^{18}O$ data from *Visser et al.* [2003]. We are grateful to Delia Oppo and an anonymous reviewer for their insightful comments and helpful suggestions; to Yvon Balut and the R/V "*Marion Dufresne*" crew for all their efforts; to Mara Weinelt for constructive suggestions; to Nadine Gehre, Karin Kissling, and Brigitte Salomon for technical help; and to H. H. Cordt, H. Gier, and H. Heckt for carefully processing the isotope analysis. This work was funded by DFG grant KU649/14-2.

References

Anand, P., H. Elderfield, and M. H. Conte (2003), Calibration of Mg/Ca thermometry in planktonic foraminifera from a sediment trap time series, *Paleoceanography*, *18*(2), 1050, doi:10.1029/2002PA000846.

Andreasen, D. J., and A. C. Ravelo (1997), Tropical Pacific Ocean thermocline depth reconstructions for the last glacial maximum, *Paleoceanography*, *12*(3), 395–413.

Ashkenazy, Y., and E. Tziperman (2006), Scenarios regarding the lead of equatorial sea surface temperature over global ice volume, *Paleoceanography*, *21*, PA2006, doi:10.1029/2005PA001232.

Bassinot, F., et al. (2002), Scientific report of the WEPAMA cruise, MD122/IMAGES VII, 453 pp., Inst. Fr. pour la Rech. et la Technol., Polaires, France.

Bé, A. W. H. (1977), An ecological, zoogeographical and taxonomic review of recent planktonic foraminifera, in *Oceanic Micropaleontology*, edited by A. T. S. Ramsay, pp. 1–100, Elsevier, New York.

Bemis, B. E., H. J. Spero, J. Bijma, and D. W. Lea (1998), Reevaluation of the oxygen isotopic composition of planktonic foraminifera: Experimental results and revised paleotemperature equations, *Paleoceanography*, *13*(2), 150–160.

Cane, M. A., and A. Clement (1999), A Role for the tropical Pacific coupled ocean-atmosphere system on Milankovitch and millennial timescales. part II: Global impacts, in *Mechanisms of Global Climate Change at Millennial Time Scales*, *Geophys. Monogr. Ser.*, vol. 112, edited by P. U. Clark, R. S. Webb, and L. D. Keigwin, pp. 373–383, AGU, Washington D. C.

Conan, S. M.-H., E. M. Ivanova, and G.-J. A. Brummer (2002), Quantifying carbonate dissolution and calibration of foraminiferal dissolution indices in the Somali Basin, *Mar. Geol.*, *182*, 325–349.

Conkright, M. E., et al. (2002), World Ocean Atlas 2001: Objective analyses, data statistics, and figures, CD-ROM documentation, *Internal Rep. 17*, 17 pp., Natl. Oceanogr. Data Cent., Silver Spring, Md.

Cortese, G., and A. Abelmann (2002), Radiolarian-based paleotemperatures during the last 160 kyr at ODP Site 1089 (Southern Ocean, Atlantic sector), *Palaeogeogr. Palaeoclimatol. Palaeoecol.*, *182*, 259–286.

Cresswell, G., A. Frische, J. Peterson, and D. Quadfasel (1993), Circulation in the Timor Sea, *J. Geophys. Res.*, *98*(C8), 14,379–14,389.

De Deckker, P., N. J. Tapper, and S. van der Kaars (2002), The status of the Indo-Pacific Warm Pool and adjacent land at the Last Glacial Maximum, *Global Planet. Change*, *35*, 25–35.

Dekens, P. S., D. W. Lea, D. K. Pak, and H. J. Spero (2002), Core top calibration of Mg/Ca in tropical foraminifera: Refining paleotemperature estimation, *Geochem. Geophys. Geosyst.*, *3*(4), 1022, doi:10.1029/2001GC000200.

de Villiers, S., M. Greaves, and H. Elderfield (2002), An intensity ratio calibration method for the accurate determination of Mg/Ca and Sr/Ca of marine carbonates by ICP-AES, *Geochem. Geophys. Geosyst.*, *3*(1), 1001, doi:10.1029/2001GC000169.

Esat, T. M., M. T. McCulloch, J. Chappel, B. Pillans, and A. Omura (1999), Rapid fluctuations in sea level recorded at Huon Peninsula during the penultimate deglaciation, *Science*, *283*, 197–209.

Godfrey, J. S. (1996), The effect of the Indonesian Throughflow on ocean circulation and heat exchange with the atmosphere: A review, *J. Geophys. Res.*, *101*(C5), 12,217–12,237.

Gordon, A. L., and R. A. Fine (1996), Pathways of water between the Pacific and Indian oceans in the Indonesian seas, *Nature*, *379*, 146–149.

Gordon, A. L., R. D. Susanto, and A. L. Ffield (1999), Throughflow within Makassar Strait, *Geophys. Res. Lett.*, *26*, 3325–3328.

Gordon, A. L., R. D. Susanto, and K. Vranes (2003), Cool Indonesian Throughflow as a consequence of restricted surface layer flow, *Nature*, *425*, 824–828.

Hastings, D., M. Kienast, S. Steinke, and A. Whitko (2001), A comparison of three independent paleotemperature estimates from a high resolution record of deglacial SST records in the tropical South China Sea, *Eos Trans. AGU*, *82*, Fall Meet. Suppl., Abstract PP12B-10.

Hemleben, C., M. Spindler, and O. R. Anderson (1989), *Modern Planktonic Foraminifera*, 363 pp., Springer, New York.

Herguera, J. C., and W. H. Berger (1991), Paleoproductivity from benthic foraminifera abundance: Glacial to postglacial change in the west-equatorial Pacific, *Geology*, *19*, 1173–1176.

Holbourn, A., W. Kuhnt, H. Kawamura, Z. Jian, P. Grootes, H. Erlenkeuser, and J. Xu (2005), Orbitally paced paleoproductivity variations in the Timor Sea and Indonesian Throughflow variability during the last 460 kyr, *Paleoceanography*, *20*(3), PA3002, doi:10.1029/2004PA001094.

Jian, Z., B. Huang, W. Kuhnt, and H. Lin (2001), Late Quaternary upwelling intensity and east Asian monsoon forcing in the South China Sea, *Quat. Res.*, *55*, 363–370.

Kienast, M., S. Steinke, K. Stattegger, and S. E. Calvert (2001), Synchronous tropical South China Sea SST change and Greenland warming during deglaciation, *Science*, *297*, 226–230.

Koutavas, A., J. Lynch-Stieglitz, T. M. Marchitto Jr., and J. P. Sachs (2002), El Niño-like pattern in ice age tropical Pacific sea surface temperature, *Science*, *297*, 226–230.

Kuhnt, W., S. Hess, and Z. Jian (1999), Quantitative composition of benthic foraminiferal assemblages as a proxy indicator for organic carbon flux rates in the South China Sea, *Mar. Geol.*, *156*, 123–158.

Kuhnt, W., A. Holbourn, R. Hall, M. Žuvela, and R. Käse (2004), Neogene history of the Indonesian Throughflow, in *Continent-Ocean Interactions Within East Asia Marginal Seas*, *Geophys. Monogr. Ser.*, vol. 149, edited by P. Clift et al., pp. 299–320, AGU, Washington, D. C.

Kuhnt, W., et al. (2006), Cruise report SONNE-185 "Variability of the Indonesian Throughflow and Australasian climate history of the last 150 000 years (VITAL)", report, Inst. für Geowiss., Christian-Albrechts-Univ. zu Kiel, Kiel, Germany, in press.

Lambeck, K., and J. Chappell (2001), Sea level change through the last glacial cycle, *Science*, *292*, 679–686.

Laskar, J. (1990), The chaotic motion of the solar system: A numerical estimate of the size of the chaotic zones, *Icarus*, *88*, 266–291.

Le, J., and N. J. Shackleton (1992), Carbonate dissolution fluctuations in the western equatorial Pacific during the late Quaternary, *Paleoceanography*, *7*(1), 21–42.

Lea, D. W., D. K. Pak, and H. J. Spero (2000), Climate impact of late Quaternary equatorial Pacific sea surface temperature variations, *Science*, *289*, 1719–1724.

Lea, D. W., D. K. Pak, L. C. Peterson, and K. A. Hughen (2003), Synchroneity of tropical and high-latitude Atlantic temperatures over the last glacial termination, *Science*, *301*, 1361–1364.

Lee, T., I. Fukumori, D. Menemenlis, Z. Xing, and L.-L. Fu (2002), Effects of the Indonesian Throughflow on the Pacific and Indian oceans, *J. Phys. Oceanogr.*, *32*(5), 1404–1429.

Liu, Z. H., and T. D. Herbert (2004), High-latitude influence on the eastern equatorial Pacific climate in the early Pleistocene epoch, *Nature*, *427*, 720–723.

Lohmann, G. P. (1995), A model for variation in the chemistry of planktonic foraminifera due to secondary calcification and selective dissolution, *Paleoceanography*, *10*(3), 445–457.

Longhurst, A. (1998), *Ecological Geography of the Sea*, Elsevier, New York.

Martin, P. A., and D. W. Lea (2002), A simple evaluation of cleaning procedures on fossil benthic foraminiferal Mg/Ca, *Geochem. Geophys. Geosyst.*, *3*(10), 8401, doi:10.1029/2001GC000280.

Martinson, D. G., et al. (1987), Age dating and the orbital theory of the ice ages: Development of a high-resolution 0 to 300,000 year chronostratigraphy, *Quat. Res.*, *27*, 1–29.

Medina-Elizalde, M., and D. W. Lea (2005), The mid-Pleistocene transition in the tropical Pacific, *Science*, *310*, 1009–1012, doi:10.1126/science.1115933.

Molcard, R., M. Fieux, and F. Syamsudin (2001), The throughflow within Ombai Strait, *Deep Sea Res., Part I*, *48*, 1237–1253.

Murray, S. P., and D. Arief (1988), Throughflow into the Indian Ocean through the Lombok Strait, January 1985–January 1986, *Nature*, *333*, 444–447.

North Greenland Ice Core Project Members (2004), High-resolution record of Northern Hemisphere climate extending into the last interglacial period, *Nature*, *431*, 147–151.

Oppo, D. W., and Y. Sun (2005), Amplitude and timing of sea-surface temperature change in the northern South China Sea: Dynamic link to the east Asian monsoon, *Geology*, *33*, 785–788, doi:10.1130/G21867.1.

Paillard, D., L. Laberyrie, and P. Yiou (1996), Macintosh program performs time-series analysis, *Eos Trans. AGU*, *77*, 39.

Potemra, J. T., S. L. Hautala, and J. Sprintall (2003), Vertical structure of Indonesian Throughflow in a large-scale model, *Deep Sea Res., Part II*, *50*, 2143–2161.

Ravelo, A. C., and R. G. Fairbanks (1992), Oxygen isotopic composition of multiple species of planktonic foraminifera: Recorders of the modern photic zone temperature gradient, *Paleoceanography*, *7*(6), 815–831.

Ravelo, A. C., R. G. Fairbanks, and S. G. H. Philander (1990), Reconstructing tropical Atlantic hydrography using planktonic foraminifera and an ocean model, *Paleoceanography*, *5*(3), 409–431.

Rosenthal, Y., and G. P. Lohmann (2002), Accurate estimation of sea surface temperatures using dissolution-corrected calibrations for Mg/Ca paleothermometry, *Paleoceanography*, *17*(3), 1044, doi:10.1029/2001PA000749.

Rosenthal, Y., G. P. Lohmann, K. C. Lohmann, and R. M. Sherrell (2000), Incorporation and preservation of Mg in Globigerinoides sacculifer: Implications for reconstructing the temperature and $^{18}O/^{16}O$ of seawater, *Paleoceanography*, *15*(1), 135–145.

Russell, A. D., B. Hönisch, H. J. Spero, and D. W. Lea (2004), Effects of seawater carbonate ion concentration and temperature on shell U, Mg, and Sr in cultured planktonic foraminifera, *Geochim. Cosmochim. Acta*, *68*(21), 4347–4361.

Saito, T., P. R. Thompson, and D. Breger (1981), *Systematic Index of Recent and Pleistocene Planktonic Foraminifera*, 190 pp., Univ. of Tokyo Press, Tokyo.

Sarnthein, M., and K. Winn (1990), Reconstruction of low and middle latitude export productivity, 30,000 years B. P. to present: Implication for control of global carbon reservoirs, in *Climate-Ocean Interaction*, edited by M. E. Schlesinger, pp. 319–342, Springer, New York.

Schiller, A., J. S. Godfrey, P. C. McIntosh, G. Meyers, and S. E. Wijffels (1998), Seasonal near-surface dynamics and thermodynamics of the Indian Ocean and Indonesian Throughflow in a global ocean general circulation model, *J. Phys. Oceanogr.*, *28*(11), 2288–2312.

Schmidt, M. W., H. J. Spero, and D. W. Lea (2004), Links between salinity variation in the Caribbean and North Atlantic thermocline circulation, *Nature*, *428*, 160–163.

Shackleton, N. J., M. Chapman, M. F. Sánchez-Goñi, D. Pailler, and Y. Lancelot (2002), The classic marine isotope substage 5e, *Quat. Res.*, *58*, 14–16.

Shackleton, N. J., M. F. Sánchez-Goñi, D. Pailler, and Y. Lancelot (2003), Marine isotope substage 5e and the Eemian interglacial, *Global Planet. Change*, *36*, 151–155.

Sirocko, F., K. Seelos, K. Schaber, B. Rein, F. Dreher, M. Diehl, R. Lehne, K. Jäger, M. Krbetschek, and D. Degering (2005), A late Eemian aridity pulse in central Europe during the last glacial inception, *Nature*, *436*, 833–836, doi:10.1038/nature03905.

Song, Q., and A. L. Gordon (2004), Significance of the vertical profile of the Indonesian Throughflow transport to the Indian Ocean, *Geophys. Res. Lett.*, *31*, L16307, doi:10.1029/2004GL020360.

Speich, S., B. Blanke, and G. Madec (2001), Warm and cold water routes of an O.G.C.M. thermohaline conveyor belt, *Geophys. Res. Lett.*, *28*(2), 311–314.

Tapper, N. (2002), Climate, climatic variability and atmospheric circulation patterns in the maritime continent region, in *Bridging Wallace's Line: The Environmental and Cultural History and Dynamics of the SE-Asian-Australian Region*, edited by P. Kershaw et al., *Adv. Geoecol.*, *34*, 5–38.

Ter Braak, C. J. F. (1995), Ordination, Chapter 5 in: *Data Analysis in Community Landscape Ecology*, edited by R. H. G. Jongman, C. J. F. Ter Braak, and O. F. R. Van Tongeren, pp. 91–173, Cambridge Univ. Press, New York.

Thunell, R., E. Tappa, C. Pride, and E. Kincaid (1999), Sea-surface temperature anomalies associated with the 1997–1998 El Niño recorded in the oxygen isotope composition of planktonic foraminifera, *Geology*, *27*, 843–846.

Visser, K., R. Thunell, and L. Stott (2003), Magnitude and timing of temperature change in the Indo-Pacific warm pool during deglaciation, *Nature*, *421*, 152–155.

Waelbroeck, C., L. Labeyrie, E. Michel, J.-C. Duplessy, J. F. McManus, K. Lambeck, E. Balbon, and M. Labracherie (2002), Sea-level and deep water temperature changes derived from benthic foraminifera isotopic records, *Quat. Sci. Rev.*, *21*, 295–305, doi:10.1016/S0277-3791 (01)00101-9.

Wang, P., S. Clemens, L. Beaufort, P. Braconnot, G. Ganssen, Z. Jian, P. Kershaw, and M. Sarnthein (2005), Evolution and variability of the Asian monsoon system: State of the art and outstanding issues, *Quat. Sci. Rev.*, *24*, 595–629.

Wollenburg, J., and W. Kuhnt (2000), The response of benthic foraminifers to carbon flux and primary production in the Arctic Ocean, *Mar. Micropaleontol.*, *40*, 189–231.

You, Y., and M. Tomczak (1993), Thermocline circulation and ventilation in the Indian Ocean derived from water mass analysis, *Deep Sea Res., Part I*, *40*, 13–56.

Žuvela, M. (2005), Modelling of the Indonesian Throughflow on glacial-interglacial timescales, Ph.D thesis, Math.-Naturwiss. Fak., Christian-Albrechts-Univ. Kiel, Kiel, Germany.

N. Andersen, Leibniz Laboratory for Radiometric Dating and Stable Isotope Research, Christian-Albrechts-University, Max-Eyth-Str. 11-13, D-24118 Kiel, Germany. (nandersen@leibniz.uni-kiel.de)

G. Bartoli, A. Holbourn, W. Kuhnt, and J. Xu, Institute of Geosciences, Christian-Albrechts-University, Olshausenstr. 40, D-24118 Kiel, Germany. (gb@gpi.uni-kiel.de; ah@gpi.uni-kiel.de; wk@gpi.uni-kiel.de; jx@gpi.uni-kiel.de)